Mesoscopic Monte Carlo Simulations of Stochastic Encounters between Photoactivated Rhodopsin and Transducin in Disc Membranes

Daniele Dell'Orco*,†,‡ and Henning Schmidt§

Department of Chemistry, University of Modena and Reggio Emilia and Dulbecco Telethon Institute, via Campi 183 41100 Modena, Italy, and Systems Biology and Bioinformatics Group, University of Rostock, Rostock, Germany

Received: October 12, 2007; In Final Form: January 9, 2008

The issue of how the molecular organization of rod outer segments (ROS) discs affects the initial timing of the photoresponse in vertebrates has been recently raised by novel structural findings that raise doubts about the classical scenario of monomeric rhodopsin (R) and heterotrimeric transducin (G) freely diffusing in the membrane milieu. In this study, we investigate this issue by means of mesoscopic Monte Carlo (MMC) simulations of the stochastic encounters between one photoactivated R and one G, explicitly taking into account the molecular size and the diffusion coefficient of each species as well as crowding effects. Three different scenarios were compared with respect to their effects on timing, namely, (a) the classical framework, where both G and monomeric R are allowed to freely diffuse in the ROS disc membrane, (b) the ideal paracrystalline organization of R dimers considered as a structural unit, where ordered rows completely cover the disc membrane patch, and (c) the scenario suggested by recent AFM data, where R dimers organize in differently sized rafts with varying local concentrations. Our simulations suggest that a similar kinetic response could arise from very different microscopic scenarios, thus opening new interpretations to the controversial recent findings. Moreover, we show that if high-density R packing on ROS discs is characterized by a highly ordered structural organization rather than unspecific aggregation, an unexpected favorable effect on the temporal response of early phototransduction reactions can occur.

Introduction

Visual phototransduction in vertebrates is the complex result of many molecular processes eventually resulting from the absorption of a photon by a photoreceptor to electrical signals in the retina. In particular, the absorption of even single photons in rod cells is conferred to rhodopsin (R), the prototypical class-A G protein coupled receptor (GPCR), which is present at high concentration in the ∼1,000 stacked discs constituting the rod outer segments (ROS).

The probability of a single photon absorption by R, leading to a photoactivated rhodopsin (R*), is increased by the R's packing in such tightly stacked ROS disc membranes.[1] The packing properties will affect the local molecular organization of membrane-associated proteins on the disc, influencing the lateral and rotational diffusion of both integral (e.g., R) and peripheral (e.g., transducin, (G)) membrane proteins in the lipid milieu. The rate of stochastic encounters between a photoactivated rhodopsin and one G protein needs to be sufficiently high in order to be able to trigger the whole phototransduction cascade that elicits fast electrophysiological responses with the high gain and amplification observed empirically.[2−5]

Molecular simulations have been performed in the past decade, which all relied on the widely accepted diffusion-limit rate framework and proved successful in predicting properties related to both activation[6−8] and recovery-deactivation[9] of the cascade. Recently, comprehensive models of vertebrate rod phototransduction were presented,[10,11] which, by means of a stochastic/deterministic approach, are capable of reproducing single-photon response behaviors as well as responses to high light levels, causing complete response saturation and/or significant light adaptation.[10] Finally, the fact that R is one of the two GPCRs for which the 3D structure has been experimentally determined[12,13] allowed for a number of structural and functional features to be inferred about the same and other similar pathways, both experimentally and by means of computational modeling approaches (see ref 14 for a review).

Despite the successful descriptions obtained so far by in vitro, in vivo, and in silico studies, some recent findings raised profound questions concerning our deep understanding of the molecular aspects related to phototransduction. The classical picture employed to interpret the molecular mechanisms, underlying the high rate of the visual response, is that of a monomeric R randomly dispersed and freely diffusing in a fluid lipid matrix.[15] This scenario has been deeply challenged by the recent results from atomic force microscopy (AFM), which revealed rows of R dimers densely packed in paracrystalline arrays (Figure 1).[16] The finding that R dimers form paracrystalline rafts that float in the bilayer has been contended;[15] however, further evidence was provided of such native organization.[17] While the formation of constitutive R dimers is difficult to reconcile with diffusion data, a paracrystalline organization seems, prima facie, incompatible with the fast lateral diffusion of R that is required in the classical framework.[18−20] In particular, the average density of R molecules in disc membranes determined by Fotiadis et al. by AFM experiments[16]

* Corresponding author. Telephone +39 059 2055024. Fax +39 059 373543. E-mail: daniele.dellorco@unimore.it.
† University of Modena and Reggio Emilia.
‡ Dulbecco Telethon Institute.
§ University of Rostock.

10.1021/jp709963f CCC: $40.75
Published on Web 03/18/2008

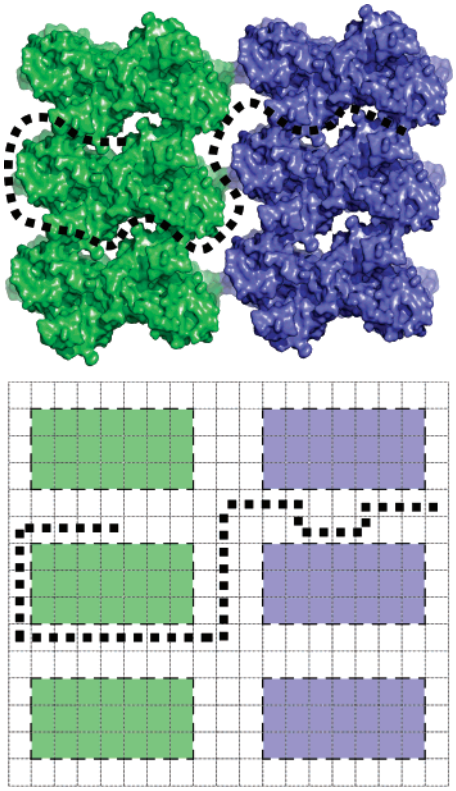

Figure 1. Six rhodopsin dimers aligned in two rows, as seen from the cytoplasmic side in a direction perpendicular to the ROS disc membrane. The first representation (top) is based on the semiempirical 3D model obtained from AFM experiments,[17] while the second (bottom) is the one employed in MMC simulations on a square lattice grid. In particular, one row of dimers is colored green, and the other one is colored slate. The lattice grid size is $\Delta x = 1$ nm. The dotted lines refer to a possible diffusion pathway of transducin as depicted in the two representations. The atomic coordinates of the structural model were obtained starting from the highest-resolution 3D model of a R monomer (PDB entry: 1u19)[23] superimposed to the semiempirical tetrameric model of R (PDB entry: 1n3m),[17] in a fashion previously described.[25] Molecular surfaces were drawn by means of the software PYMOL 0.97 (http://pymol.sourceforge.net/).

was 48,300 μm^{-2}, which is almost double compared to the previously estimated concentration of 25,000 μm^{-2}.[5]

In this study, we address the issue of how the molecular organization of ROS discs may affect the timing of the photoresponse, by explicitly simulating a patch of disc membrane in which the classical and the recently emerged frameworks are compared by means of mesoscopic Monte Carlo (MMC) simulations. The stochastic encounters between one R* and one G were simulated by explicitly taking into account molecular sizes and diffusion coefficients of the species, as well as a number of different concentrations, affecting the crowding of the membrane patch. In detail, three different scenarios were probed: (a) the classical framework,[15,18,21] where both G and monomeric R are allowed to freely diffuse in the ROS disc membrane (Figure 2A); (b) the ideal paracrystalline organization of R dimers, considered as a structural unit, where ordered rows completely cover the disc membrane patch (Figures 1−2B); (c) the scenario suggested by recent AFM data,[16,17] where R dimers would organize in differently sized rafts with varying local concentrations, thus leaving some purely lipidic areas on the disc surface (Figure 2C).

Our simulations suggest that a similar kinetic response could arise from very different microscopic scenarios, thus opening

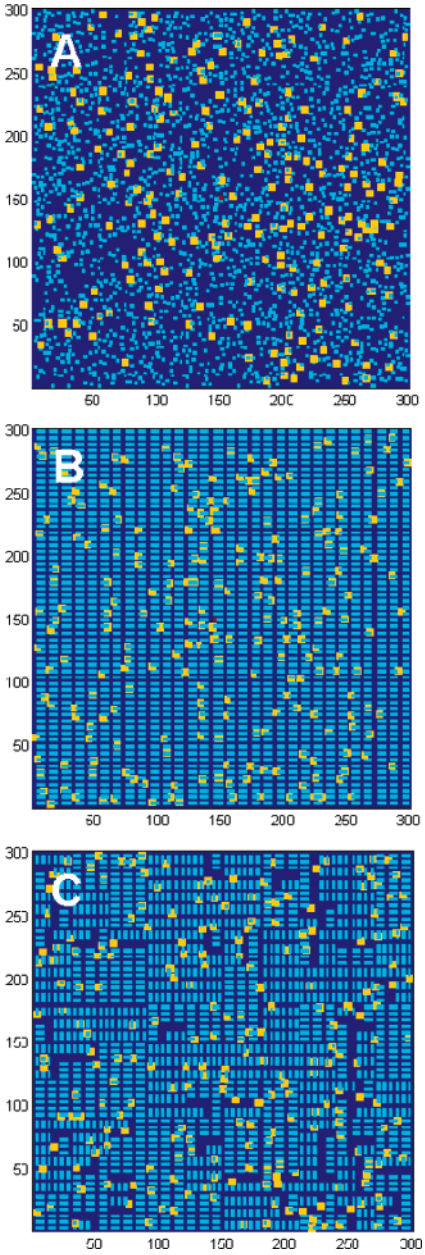

Figure 2. Snapshot of the three different lattice frameworks employed in MMC simulations on a 300 nm × 300 nm grid, as seen from the bottom view (opposite to the extradisc region of G's). (A) The classical framework, where both R's (light blue squares) and G's (yellow squares) are free to diffuse in the ROS disc patch. Dark blue areas correspond to protein-free purely lipidic zones. Here $C_R = 25{,}000\ \mu m^{-2}$, whereas $C_G = 2{,}500\ \mu m^{-2}$ like in the other panels. (B) The whole paracrystalline framework, where R dimers are aligned in rows completely covering the lattice, corresponding to $C_R = 40{,}000\ \mu m^{-2}$. (C) The framework of R-dimers placed in rafts of heterogeneous size and shape (see Methods). Here $C_R \sim 37{,}000\ \mu m^{-2}$. In all the cases, the photoactivated R is placed in the middle of the lattice and marked with a red dot.

new interpretations to the controversial recent findings. Moreover, we show that if high-density R packing on ROS discs is characterized by a highly ordered structural organization, rather than unspecific aggregation, an unexpected favorable kinetic effect could be observed. More specifically, when the effective diffusion coefficient is completely attributed to G, some kinetic advantage is observed for highly packed, highly ordered R dimers vs freely diffusing, randomly distributed monomers, at least in the dim-flash regime.

Methods

Setting the 2D Lattice for Mesoscopic Representation of a ROS Disc Membrane Patch. MMC simulations were realized employing a bidimensional (2D) square lattice, similarly to previous work.[6−9] Nevertheless, in order to account for the actual size of each molecule, our grid size was chosen to be $\Delta x = 1$ nm, which results in a considerably finer grid compared to previous work. The number of lattice points was varied from $N_x = 100$ to $N_x = 300$ points, finally leading to the choice of the latter value in all the simulations. Indeed, in view of the average diameter of ROS discs, ~ 1 μm,[17,22] simulating a 300 nm $\times$ 300 nm patch may represent a reasonable compromise between computational speed and proper size to capture enough biologically relevant information. Finally, such a lattice size also allows avoiding edge effects that increase with decreasing lattice size. The time step to be used for our simulations is determined by the grid size and the maximum diffusion constant to be simulated through the Einstein relation (see eq 1). Here we chose $\Delta t = 0.1$ μs, allowing us to correctly simulate diffusion constants up to $D_{max} = 1/4(\Delta x)^2/\Delta t = 2.5$ μm^2 s^{-1}.

To simulate the lateral diffusion of both integral (R) and peripheral (G) membrane proteins in the disc milieu, we explicitly took into account the actual molecular size of the diffusing portion of each molecule on the disc membrane. However, we further considered the presence of the remaining part of each molecule in order to avoid any unphysical interpenetration that may occur either in the membrane or in the extra-disc milieu. In detail, for R monomers, we took advantage of the crystal structure recently resolved at 2.2 Å (PDB entry: 1u19),[23] whereas, for R dimers and their putative organization in paracrystalline rows, we considered the semiempirical structural model of oligomeric R built upon AFM experiment results.[17] As for G, we considered its geometrical features as assessed from a 2.0 Å crystal structure (PDB entry: 1got).[24] The structural features of these molecules were discussed in detail previously.[25] In order to simulate the system, we needed to translate the high-resolution 3D information from the molecular models into the context of our 2D-lattice with a fixed grid size of $\Delta x = 1$ nm. In detail, (a) R monomers were represented by 3 nm $\times$ 3 nm squares, approximately accounting for the actual diameter of R; (b) G heterotrimers were represented by 6 nm $\times$ 6 nm squares for what concerns their extra-disc portion and 1 nm $\times$ 1 nm squares for what concerns their actually diffusing lipidic milieu, consisting of the farnesyl and myristoyl chains anchoring the protein to the membrane; (c) R dimers were represented by 3 nm $\times$ 7 nm rectangles, which constituted the structural unit both for the paracrystalline and the rafts frameworks (see Figure 1). In particular, the paracrystalline structure is characterized by rows of dimers uniformly separated from each other and built according to the distances assessed from the AFM semiempirical model, resulting in rectangles spaced 2 nm in the vertical direction (intra-row distance between dimers) and 3 nm in the horizontal direction (inter-row distance) (Figure 1). In order to properly cover the whole 2D lattice with paracrystalline rows of dimers, an average C_R of 40,000 μm^{-2} was necessary (Figure 2B). This concentration is in contrast to the 48,300 reported by Fotiadis et al.,[16] and is due to the fact that we used a lattice grid size of 1 nm^2, which did not allow us to model the exact molecular sizes and inter- and intra-row distances. However, we had to seek a compromise between realistic representation and computational feasibility, since, for decreasing grid size, the computational demand is exploding. As for the rafts framework, some assumptions were necessary to set up the lattice. On the basis of very recent cryoelectron tomography measurements of murine retina,[26] the distribution of R dimers is heterogeneous, R's being organized in regions of high and low density. In particular, the rafts observed presented a somewhat heterogeneous area, ranging from about 200 nm^2 up to 1,800 nm^2, with an average area of about 920 nm^2 (Paul S. H. Park, personal communication, School of Medicine, Case Western Reserve University). On the basis of these experimental data, we could define some building blocks for randomly generated rafts of reliable size. Hence, we chose three main types of building blocks: (a) small 10 nm $\times$ 15 nm rafts, each containing three vertically lined-up dimers and the relative free lipid space, corresponding to one row represented in Figure 1; (b) big 40 nm $\times$ 45 nm rafts, each containing 4 rows of 9 dimers and the relative free lipid space; (3) average sized 30 nm $\times$ 30 nm rafts, corresponding to three rows of six dimers. In order to account, at least partially, for the potentially random angular distribution of rafts on the ROS disc, the same building blocks were allowed to be placed either vertically or horizontally in the lattice grid. The resulting six types of building blocks were randomly placed in the lattice at each simulation so as to generate both R rafts of heterogeneous shape and size and R-free areas corresponding to purely lipidic patches (see Figure 2C).

Initial Amounts of R and G in Each Tested Framework. In each simulation, a number of both R and G concentrations were probed (see Results and Tables 1−4) which correspond to different initial amounts of G and R molecules to be placed in the lattice, explicitly taking into account their geometrical size and the progressive lattice occupancy. In particular, (a) in the classical framework, the proper amounts of R's and G's were randomly placed in the lattice at each simulation start; (b) in the case of paracrystalline organization, the lattice was initially set with R dimers, placed as described, followed by random positioning of the proper amounts of G's; (c) in the case of dimeric R-rafts, R's were placed as described, followed by random positioning of the proper amounts of G's.

In all cases, the single photoactivated R* was placed in the middle of the lattice in order to minimize potential edge effects. In the classical case, R* was allowed to diffuse, while it remained fixed in the two other cases.

The initial amounts of R and G and their diffusion coefficients employed in this study refer to amphibian rods at room temperature, similarly to previous work.[7] Slightly different values were reported for mammalian rods, which resulted in an average encounter rate of $\sim$16,000 s^{-1} for mammalian rods at body temperature, whereas for amphibian rods it was found to be $\sim$6,000 s^{-1}.[5]

Stochastic Simulations of Lateral Diffusions in the Diffusion-Limited Rate Hypothesis. In all the three frameworks investigated by MMC simulations, the diffusion-limit rate is assumed, that is, the first occurring molecular contact between R* and a G leads to G protein activation. Moreover, we explicitly assumed that diffusion is the only physical means of transportation and interaction between molecules, and thus the only one responsible for the observed kinetics. Therefore, any other physical interaction, such as electrostatic forces between R and R/R*, R/R* and G, or G and G, which may contribute to the observed rates, were neglected in this work. This appears reasonable considering the limited space resolution of the model that, similarly to previous work,[6−8] does not allow for a reliable analysis of such effects.

In our simulations, each diffusible species was allowed to move in the lattice either in vertical or horizontal direction at each time step Δt, according to a Monte Carlo criterion, unless the lattice points, corresponding to the move, were occupied

by another molecule. Similarly to what was previously done by other researchers,[7,8] we could convert the continuous case of a molecule diffusing in two dimensions with an ideal diffusion coefficient D (diffusion coefficient at infinite dilution) into the square-lattice representation. For the continuous case, the expected mean-square distance $\langle r^2 \rangle$ traversed by such a molecule in the time t is given by the Einstein relation:

$$\langle r^2 \rangle = 4Dt \tag{1}$$

In the square lattice, with spacing Δx and for a time increment Δt, the simulated diffusion coefficient can be shown to be

$$D = D_{\max} p_{\text{move}} \tag{2}$$

where $D_{\max}$ is given by $1/4(\Delta x)^2/\Delta t$, and p_{move} is the probability that a molecule moves within a time-step of duration Δt to any one of the four nearest orthogonal locations in the lattice. As discussed above, we chose the lattice grid size and the maximum diffusion coefficient to be simulated and used this relation to determine the simulation time-step. For each molecule, a pseudorandom number x_{rand} was generated in the [0,1] interval and used to define a factor f, defined as follows:

$$f = 4 \frac{x_{\text{rand}}}{p_{\text{move}}} \tag{3}$$

If $f < 4$, that is, if $x_{\text{rand}} < p_{\text{move}}$, the molecule was allowed to move randomly into an unoccupied lattice position in one of the four orthogonal directions; otherwise the move was rejected. If all four positions were already occupied by other molecules, the move was also rejected. In summary, by setting the diffusion coefficients D, one directly modifies the p_{move} for each particle.

It is well-known that the diffusion coefficient of any species is concentration-dependent,[27] and that it can, under crowding conditions, differ significantly from its value at infinite dilution. In order to compare the ideal diffusion coefficient D with its value assessed by simulation, we built an indexed lattice whose middle elements only were tracked for diffusion coefficient calculations by means of eq 1. For the diffusible species (G or G and R), diffusion coefficients D_m's were estimated by determining the mean-square diffusion lengths, corresponding to fixed time ranges. In contrast to previous work,[7,8] where p_{move} was corrected in order to obtain $D_m = D$, we will compare the ideal diffusion coefficient D with the estimated one D_m, and attribute the difference to the effect that molecular crowding has on diffusion.

Sampling of Encounter Time τ_{R^*G} and Algorithm Implementation. Each simulation was set up as described and stopped as soon as the first encounter between a G molecule and the only R* happened. The number of time steps making up the encounter time $\tau_{R^*G_i}$ was collected, and the simulation was repeated N_{sim} times to obtain the average

$$\langle \tau_{R^*G} \rangle = \frac{1}{N_{\text{sim}}} \sum_{i=1}^{N_{\text{sim}}} \tau_{R^*G_i} \tag{4}$$

and the standard error δ:

$$\delta = \frac{\sigma_{\langle \tau_{R^*G} \rangle}}{N_{\text{sim}}^{1/2}} \tag{5}$$

A number of different values for N_{sim} were tested, finally leading to the choice of $N_{\text{sim}} = 1{,}000$ for all the analyses. Indeed, this value represents a good compromise between computational time and good statistical sampling. As for the cases where D_m's were calculated, N_{sim} was varied in the range 50−1000 (see Results).

TABLE 1: Effects of Diffusion Coefficients Tuning on R*−G Encounter Time in the Freely Diffusing Framework at $T = 22$ °C[a]

D_R ($\mu m^2 s^{-1}$)[b]	D_G ($\mu m^2 s^{-1}$)[c]	τ_{R^*G} (μs)[d]
0.1	1.8	32.73 ± 1.53
0.2	1.7	31.17 ± 1.43
0.4	1.5	28.92 ± 1.29
0.6	1.3	31.61 ± 1.35
0.7[e]	1.2	29.98 ± 1.39
0.8	1.1	32.74 ± 1.59

[a] In each simulation, $C_R = 25{,}000\ \mu m^{-2}$ and $C_G = 2{,}500\ \mu m^{-2}$. [b] Ideal diffusion coefficient of monomeric rhodopsin. [c] Ideal diffusion coefficient of heterotrimeric transducin. [d] Encounter time between one photoactivated rhodopsin and one transducin molecule estimated from MMC simulations. The standard error is reported. [e] Values representing classical estimates normally used in previous simulations. See, for instance, refs 6 and 7.

The CPU time was found to vary significantly, depending on the simulation settings, such as the concentrations and diffusion coefficients of the molecular species. As an indicative value, 1,000 simulations on a 300 nm × 300 nm grid with $C_R = 25{,}000\ \mu m^{-2}$ and $C_G = 2{,}500\ \mu m^{-2}$ in the classical framework and with classical diffusion coefficients took about 48 h on a 2.4 GHz AMD Opteron Processor 150 with 1 GB RAM. Instead, when C_R was raised to 60,000 μm^{-2} and C_G was kept fixed at 2,500 μm^{-2}, the computations took about 340 h.

The code for performing MMC simulations was written in MATLAB version 7 (R14). In order to speed up the simulations, some of the functions were written in C and interfaced with MATLAB by means of suitable MEX-functions. The code is available for academic use upon request to the authors.

Results

Freely Diffusing Molecules: Effects of Diffusion Coefficients Tuning on the R*−G Encounter Time. The first scenario investigated is that of R and G freely diffusing in the ROS disc membrane milieu, according to the classical diffusion-limited framework (Figure 2A).[3,4] The effects of D_G and D_R tuning on the encounter time τ_{R^*G} were investigated at the classical ROS concentrations $C_R = 25{,}000\ \mu m^{-2}$ and $C_G = 2{,}500\ \mu m^{-2}$. Table 1 reports the values of τ_{R^*G} where, respectively, D_R was tuned from 0.1 to 0.8 $\mu m^2\ s^{-1}$ and D_G was tuned from 1.8 to 1.1 $\mu m^2\ s^{-1}$. All the runs were set so that the overall diffusion coefficient $D_{tot} = D_R + D_G$ remained fixed at 1.9 $\mu m^2\ s^{-1}$. Within the standard errors, all the simulations converged to an average τ_{R^*G} of 31.19 μs, which is fairly consistent with the value reported in the same table (29.98 ± 1.39 μs) and representing the classical conditions $D_G = 1.2\ \mu m^2\ s^{-1}$ and $D_R = 0.7\ \mu m^2\ s^{-1}$. This finding is consistent with previous theoretical arguments[3,7,8] pointing to the importance of the effective lateral diffusion coefficient defined as the sum of the D's of the diffusing species in setting the overall kinetic response.

Moreover, estimates of the diffusion coefficients (D_m's, see Methods section) from 1,000 MMC simulations led to results comparable to the ideal values for both R and G. For example, when the ideal diffusion coefficients were set to $D_R = 0.1\ \mu m^2\ s^{-1}$ and $D_G = 1.8\ \mu m^2\ s^{-1}$ we obtained, respectively, $D_{Rm} = 0.080 \pm 0.003\ \mu m^2\ s^{-1}$ and $D_{Gm} = 1.17 \pm 0.04\ \mu m^2\ s^{-1}$.

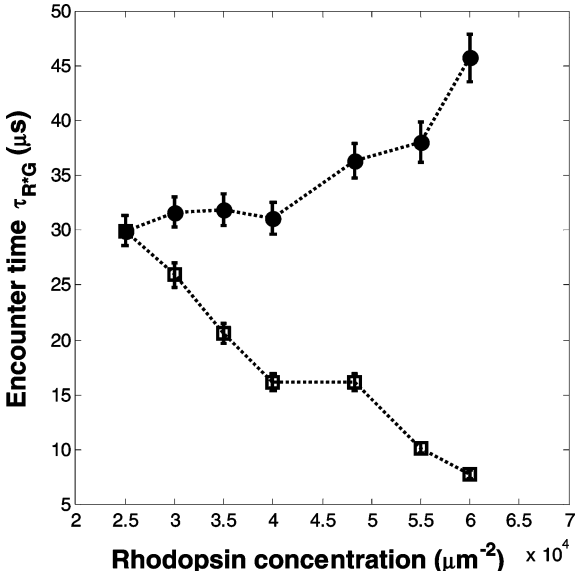

Figure 3. Crowding effects in the classical framework, with ideal diffusion coefficients set to $D_G = 1.2\ \mu m^2\ s^{-1}$ and $D_R = 0.7\ \mu m^2\ s^{-1}$. In the first case, with data points marked by filled circles, C_G was kept fixed to 2,500 μm^{-2} whereas C_R was increased up to 60,000 μm^{-2}. In the second case, with data points marked by open squares, both C_G and C_R were subsequently increased, yet with a fixed concentration ratio ($C_R/C_G = 10$).

TABLE 2: Effects of Macromolecular Crowding on R*−G Encounter Time in the Freely Diffusing Framework at T = 22 °C[a]

C_G (μm^{-2})	C_R (μm^{-2})	C_R/C_G	τ_{R^*G} (μs)
2,500	25,000	10	29.98 ± 1.39
3,000	30,000	10	25.95 ± 1.15
3,500	35,000	10	20.59 ± 0.95
4,000	40,000	10	16.11 ±0.74
4,830	48,300	10	16.16 ± 0.80
5,500	55,000	10	10.10 ± 0.48
6,000	60,000	10	7.67 ± 0.36
2,500	30,000	12	31.71 ± 1.40
2,500	35,000	14	31.91 ± 1.45
2,500	40,000	16	31.14 ± 1.41
2,500	48,300	19.3	36.39 ± 1.53
2,500	55,000	22	38.11 ± 1.83
2,500	60,000	24	45.79 ± 2.11

[a] In each simulation, $D_R = 0.7\ \mu m^2\ s^{-1}$ and $D_G = 1.2\ \mu m^2\ s^{-1}$.

Freely Diffusing Molecules: Crowding Effects on the R*−G Encounter Time. The effects of macromolecular crowding on the kinetics of R*−G encounters in the classical framework were investigated in two different ways (Table 2, Figure 3). In the first case, for each simulation, the ratio between the concentration of R and G was maintained at 10, whereas in the second case C_G was kept fixed at its classical value (C_G = 2,500 μm^{-2}). In both cases, C_R was gradually increased from its classical value (25,000 μm^{-2}) up to 60,000 μm^{-2}, hence significantly contributing to enhance the crowding of the ROS disc membrane.

The results of MMC simulations are plotted in Figure 3 and show trends in line with those expected by theoretical analysis.[27] By the law of mass action, the simultaneous increase in the concentration of both R and G will increase the reaction rate, whereby a roughly linear decrease of τ_{R^*G} is expected as the major effect. This is indeed what was observed in the first case (Table 2, Figure 3). However, when C_G was kept fixed at 2,500 μm^{-2} and C_R was subsequently increased up to 60,000 μm^{-2}, a competition between two opposite phenomena was clearly observed (Figure 3). On one hand, according to the law of mass action, τ_{R^*G} is expected to decrease with increases in C_R. On the other hand, increased crowding will cause τ_{R^*G} to increase with increasing C_R. In fact, while in the first case the concentration of both molecules is simultaneously increased, hence reasonably reducing the mean walk length before R* can find and bind any G, in the second case, an increased amount of inactive R is not balanced by increased G concentration, and therefore results in a significantly enhanced crowding. Such enhanced crowding would be expected to significantly lower the effective diffusion coefficients. Accordingly, a direct estimate of the diffusion coefficients for the case C_R = 55,000 μm^{-2} from 50 MMC simulations led to significantly lowered diffusion coefficients: $D_{Rm} = 0.30 \pm 0.04\ \mu m^2\ s^{-1}$ and $D_{Gm} = 0.59 \pm 0.09\ \mu m^2\ s^{-1}$ compared to $D_R = 0.7\ \mu m^2\ s^{-1}$ and $D_G = 1.2\ \mu m^2\ s^{-1}$.

TABLE 3: Effects of G Diffusion Coefficient Tuning on R*−G Encounter Time in the Framework of Paracrystalline Organization of R Dimers, at T = 22 °C[a]

D_G ($\mu m^2 s^{-1}$)[b]	D_{Gm} ($\mu m^2 s^{-1}$)[c]	τ_{R^*G} (μs)[d]	$\tau_{R^*Gclass}$ (μs)[e]
1.2	0.77 ± 0.08	40.37 ± 2.45	
1.5		34.27 ± 1.90	
1.7		27.97 ± 1.40	
1.9	1.21 ± 0.12	22.58 ± 1.24	47.37 ± 2.30

[a] In Each simulation, $D_R = 0\ \mu m^2\ s^{-1}$ and $C_G = 2{,}500\ \mu m^{-2}$. [b] Ideal diffusion coefficient of heterotrimeric transducin. [c] Diffusion coefficient of transducin as estimated by 100 MMC simulations with standard error. [d] Encounter time between one photoactivated rhodopsin within a random dimer and one transducin molecule estimated from MMC simulations. The standard error is reported. [e] Encounter time estimated with the same setting as in the paracrystalline framework but referring to the case of randomly distributed rhodopsins prevented to diffuse. In this case, the diffusion coefficient estimated by MMC simulation is $D_{Gm,class} = 0.84 \pm 0.13\ \mu m^2\ s^{-1}$

Our findings are consistent with the earlier studies from Saxton and Owicky[27] and similarly suggest the existence of optimum concentrations of R and G around the putative physiological values C_R = 25,000 μm^{-2} and C_G = 2,500 μm^{-2} (Figure 3, Table 2).

Paracrystalline Organization of R Dimers: Effects of G Diffusion Coefficient Tuning and Diffusion Anisotropy on R*−G Encounter Time. The second scenario probed by MMC simulations is the ideal case of R dimers densely packed on the ROS disc membrane to make up an overall paracrystalline framework (Figures 1 and 2B). While the formation of constitutive R dimers is difficult to reconcile with diffusion data, a paracrystalline organization seems incompatible with the fast lateral diffusion of R required in the traditional framework.[18−20] At the time scale of our MMC simulations, it thus was reasonable to set D_R to zero.

We performed several simulations, in which we investigated the impact that different choices of D_G had on the effective diffusion coefficient and the encounter time of G and R*. Hereby, D_G was chosen to represent the overall D_{tot}. The other parameters were fixed at $D_R = 0\ \mu m^2\ s^{-1}$ and $C_G = 2{,}500\ \mu m^{-2}$. Table 3 summarizes the results of the MMC simulations. Interestingly, when the diffusion coefficient classically attributed to G ($D_G = 1.2\ \mu m^2\ s^{-1}$) was employed, simulations converged to τ_{R^*G} = 40.37 ± 2.45 μs. However, when the effective diffusion coefficient was completely attributed to G ($D_G = D_{tot} = 1.9\ \mu m^2\ s^{-1}$), the encounter time almost halved, becoming $\tau_{R^*G} = 22.58 \pm 1.24\ \mu s$. The effects of tuning D_G in a reliable range of values within D_{tot} confirmed a striking linear correlation between τ_{R^*G} and D_G (correlation coefficient R = 0.99, Table 3).

TABLE 4: Effects of G Diffusion Coefficient Tuning on R*−G Encounter Time in the Framework of Organized Rafts of R Dimers, at $T = 22$ °C[a]

set of simulations[b]	τ_{R^*G} (μs) ($D_G = 1.2\ \mu m^2 s^{-1}$)	τ_{R^*G} (μs) ($D_G = 1.9\ \mu m^2 s^{-1}$)
1	38.76 ± 2.02	27.14 ± 1.42
2	20.99 ± 1.43	23.70 ± 1.33
3	31.01 ± 1.91	19.37 ± 1.13
4	39.78 ± 2.10	19.33 ± 1.06
5	39.74 ± 2.10	25.06 ± 1.39
6	46.60 ± 2.51	27.49 ± 1.41
7	38.76 ± 2.12	23.29 ± 1.28
8	40.02 ± 2.01	25.82 ± 1.33
9	37.89 ± 2.18	27.43 ± 1.40
10	43.03 ± 2.22	25.56 ± 1.53

[a] In Each simulation, $D_R = 0\ \mu m^2\ s^{-1}$ and $C_G = 2{,}500\ \mu m^{-2}$. [b] Each set is referred to 1,000 MMC simulations done in the same initial framework, keeping the same distribution of R-dimers rafts and randomly distributing G's. From one set of simulations to another one, the rafts' disposition was randomly changed, hence leading to a different R's distribution. See the Methods section.

In order to allow for a direct comparison between the paracrystalline framework and the classical one with freely diffusing monomeric R's, we performed a simulation where R's and G's were randomly distributed over the lattice with the same concentrations ($C_R = 40{,}000\ \mu m^{-2}$, $C_G = 2{,}500\ \mu m^{-2}$). The diffusion coefficients were also kept the same ($D_R = 0\ \mu m^2\ s^{-1}$, $D_G = 1.9\ \mu m^2\ s^{-1}$), thus D_G accounted for the overall diffusion coefficient. Interestingly, the encounter time roughly doubled compared to the paracrystalline case, that is, $\tau_{R^*G} = 47.37 \pm 2.30\ \mu s$. In this respect, also significant is the fact that the estimated diffusion coefficient of G in this case ($D_{Gm} = 0.84 \pm 0.13\ \mu m^2\ s^{-1}$) is significantly reduced compared to the case of paracrystalline organization ($D_{Gm} = 1.21 \pm 0.12\ \mu m^2\ s^{-1}$). This suggests that the anisotropic and "more ordered" diffusion pathway imposed to G by the paracrystalline organization of R dimers might be kinetically favorable, at least within this specific setting.

Rafts of Organized R Dimers: Effects of G Diffusion Coefficient Tuning and Diffusion Anisotropy on R*−G Encounter Time. The organization of R dimers in rafts on the ROS disc membrane, as suggested by AFM data[16,17] was investigated by MMC simulations in order to probe the effects of such structural framework on the R*−G encounter time. In these simulations, the randomness of both the rafts' disposition and size in the lattice on one hand, and the randomness of G distribution on the other prompted us to repeat each set of 1,000 MMC samplings 10 times, by sampling at least 10 randomized raft distributions for each set. Under the same assumptions as in the paracrystalline framework, we prevented diffusion of R dimers by setting $D_R = 0\ \mu m^2\ s^{-1}$ in each case.

Two different diffusion coefficients for G were probed: the classical value $D_G = 1.2\ \mu m^2\ s^{-1}$ and the effective diffusion coefficient $D_G = 1.9\ \mu m^2\ s^{-1}$. Results are reported in Table 4 and Figure 4. When the classical G diffusion coefficient ($D_G = 1.2\ \mu m^2\ s^{-1}$) was employed, a significantly greater dispersion of τ_{R^*G}'s was observed compared to the case when $D_G = D_{tot} = 1.9\ \mu m^2\ s^{-1}$ was used (Figure 4). About 60% of the estimated encounter times is approximately 40 μs for $D_G = 1.2\ \mu m^2\ s^{-1}$, while about 80% of τ_{R^*G}'s is approximately 25 μs for $D_G = 1.9\ \mu m^2\ s^{-1}$. The higher homogeneity of the second case is highlighted by its roughly halved standard deviation ($\sigma_{1.9} = 3.03\ \mu s$) compared to the first one ($\sigma_{1.2} = 7.05\ \mu s$). In line, the average encounter times significantly differ from one another, being $\langle \tau_{R^*G_{1.2}} \rangle = 37.66\ \mu s$ and $\langle \tau_{R^*G_{1.9}} \rangle = 24.42\ \mu s$. We point out that the discrepancy (δ) between these values and that from the classical diffusion framework, in which $\tau_{R^*G} = 29.98 \pm 1.39\ \mu s$, is similar in magnitude, although in the first case it is slightly higher ($\delta_{1.2} = 7.6\ \mu s$ and $\delta_{1.9} = -5.6\ \mu s$). Finally, in the two cases the estimated G diffusion coefficients were, respectively, $D_{Gm} = 0.75 \pm 0.11\ \mu m^2\ s^{-1}$ for $D_G = 1.2\ \mu m^2 s^{-1}$, and $D_{Gm} = 1.23 \pm 0.17\ \mu m^2\ s^{-1}$ for $D_G = 1.90\ \mu m^2 s^{-1}$.

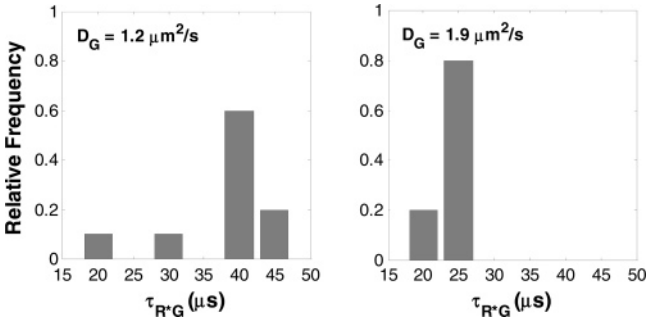

Figure 4. Histograms reporting the distribution of encounter times τ_{R^*G}'s for two different G diffusion coefficients in the framework of randomly sized and shaped rafts of R dimers. In the left panel, the "classical" ideal G diffusion coefficient was set, that is $D_G = 1.2\ \mu m^2\ s^{-1}$, whereas, in the right panel, the overall effective diffusion coefficient was attributed to G, that is, $D_G = 1.9\ \mu m^2\ s^{-1}$. In both cases, R dimers were considered immobile, that is, $D_R = 0\ \mu m^2\ s^{-1}$.

Discussion

All the MMC simulations performed in this study focused on the first encounter between one R* and G in the ROS disc membrane. In principle, it is possible to extend the investigation to the presence of more R*'s in the same patch, using the same computational approach presented here. Furthermore, it would also be possible to follow events subsequent to the first encounter of R*−G. This would increase the extent to which results from such simulations may account for the salient features of electrophysiological responses. Moreover, with a corresponding increase in computational time, it could be possible to explicitly simulate the presence of other membrane-associated molecules with high molecular weight, such as phosphodiesterase, the R9AP-RGS9-Gβ5 complex, and guanylate cyclase, which might be relevant to the issues related to crowding. The presence of such molecules was neglected in this study, which solely aimed to compare the timing effects in the three frameworks where R* and G binding may occur. However, despite the low concentration of these peripheral membrane proteins compared to R and G, their effective area may influence to some extent the diffusion of R/R* and G, and therefore the resulting τ_{R^*G}. This specific point needs further analysis that is intended in future research.

Our results highlight some interesting differences between the three conjectured frameworks when considering the kinetic response associated with the stochastic collisions between R* and G, and further disclose unexpected similarities. The classical scenario is based upon the earlier observations that both the proteins diffuse in the lipid milieu and the frequency of collisional encounters ν_{R^*G} sets the speed of phototransduction.[3,7,8,28,29] In particular, it can be shown[3,29] that this frequency is time-dependent. However, in a time range of about 5−500 ms, its variability is quite modest, and for times greater than 50 ms it can be well approximated as follows:

$$\nu_{R^*G} \leq 1.5\,(D_R + D_G)C_G \qquad (6)$$

Although referring to time intervals that greatly exceed the time range concerning the events analyzed in our simulations (i.e.,

tens of microseconds), this relation has a wide physiological relevance as the amplification constant of the whole visual cascade depends directly on ν_{R^*G}, at least at times on the order of 50 ms.[28] However, while early measurements of D_R were reported[18−20] and are compatible with a value of $D_R = 0.7\ \mu m^2\ s^{-1}$,[30] to our knowledge no direct experimental measurement of either rotational or lateral diffusion coefficient of G was ever reported. Indeed, all the mathematical models built by means of eq 6 and the associated assumptions are based on an estimated value for D_G of 1.2 $\mu m^2\ s^{-1}$.[3,5] Moreover, although both C_G and C_R were experimentally measured,[31] the average density of R molecules in disc membranes recently determined by Fotiadis et al.[16] was 48,300 μm^{-2}, which is almost the double value compared to the previously measured value of 25,000 μm^{-2}.[5] Hence, it is important to keep in mind that the interpretations of many in vitro and in vivo data, as well as the successful mathematical models built based on eq 6, indeed rely on quantities whose values are either unmeasured (D_G) or under active reevaluation (D_R and C_R).

Whereas the presence of constitutive dimers of R on the disc membrane is difficult to reconcile with diffusion data, a paracrystalline organization (with rafts of R dimers) would seem to be incompatible with the fast lateral diffusion of R that is assumed in the classical framework.[18−20] In fact, such incompatibility between the first framework on one hand and the second and the third on the other is apparent and has been the object of debates.[15] However, while the importance of both R and G diffusion coefficients in achieving the correct time-response for the first R*−G encounter was demonstrated in our study (Table 1) and the crowding effects (Table 2 and Figure 3) were found to be consistent with earlier observations by Saxton and Owicki,[27] our simulations clearly suggest that similar kinetic responses, in terms of the τ_{R^*G} values, can be obtained despite very different assumptions concerning the structural features of the ROS disc membrane. In this respect, modeling the paracrystalline framework allowed us to test the effects of both diffusion coefficient and variations in anisotropy on G diffusion in a highly ordered milieu composed of putative immobile R dimers. While the classically estimated $D_G = 1.2\ \mu m^2\ s^{-1}$ significantly slows down the encounter process and therefore the response (Table 3), assigning the effective diffusion entirely to G ($D_G = 1.9\ \mu m^2\ s^{-1}$) considerably speeds the R*−G encounters (Table 3). We point out that the same assumptions regarding diffusion coefficients and concentrations adopted in the classical framework lead to dramatically enhanced encounter rates (i.e., decreases in τ_{R^*G}; Table 3) in the nonclassical scenarios. Therefore, our simulations reveal the counterintuitive result that a highly organized paracrystalline structure might favorably affect the collision frequency, even at very high R concentrations (∼40,000 R μm^{-2}) as estimated by Fotiadis et al.[15]

Particularly interesting are the results concerning the differently sized rafts of R dimers, which clearly show that the attribution of the overall effective diffusion coefficient to G leads to a somewhat compact distribution of τ_{R^*G} (Table 4, Figure 4), with an average value not far from the classical one, i.e., $\tau_{R^*G} \sim 30\ \mu s$. Overall, these results confirm that the physiological picture arising from eq 6, at least for the parts strictly dependent on R and G, could be obtained through very different microscopic scenarios and that it is sufficient to tune D_G to obtain sufficiently fast responses even at high concentrations of immobile R. This last inference gains a particular meaning in light of the lack of any actual experimental measurement of D_G.

A very recent in vivo study[32] on a mutated form of G lacking the N-terminal acylation sequence, constituting the major lipophilic anchor of the G protein, highlighted severe defects in the cellular localization of G. However, only a 3-fold decrease in the amplification constant was observed,[32] which could be interpreted as an increase of G lateral diffusion, despite the residual presence of the farnesyl moiety at the Gγ −C terminal.[32] Hence, there could be several factors that are able to modulate D_G, which could affect the whole photoresponse, and perhaps a revision of the putative value attributed to D_G, which has never been measured, would be necessary in light of recent findings, and since its estimate is yet widely employed in a number of mathematical models.[3,6−9,29,33,34]

Our results could also partially help in interpreting some of the controversial findings concerning the putative functional role of R dimers. Transmission electron microscopy on lipidic micelles containing R in its monomeric, dimeric, and paracrystalline states showed that, although both photoactivated R monomers and R dimers are capable of activating G, the activation is much faster when R exists as dimers, at least in vitro.[34] Moreover, docking simulations[25,36] showed that the essential molecular determinants for G recognition are contained in one R monomer, independent of its oligomeric state. Collectively, these findings are kinetically consistent with our results, suggesting some kinetic advantage of highly packed, highly ordered R dimers vs freely diffusing, randomly distributed monomers, at least in the dim-flash regime. In this respect, the recent studies focusing on highly packed R in polyunsaturated membranes[37] and inferring that a high R packing would lower visual transduction by retarding lateral diffusion and reducing the active form of R should be considered in light of the "order level" of such packing, which in turn may influence the isotropy of G diffusion. In fact, we clearly showed that, when starting from the same concentration and ideal G diffusion coefficient, an ordered R-packing (a paracrystalline framework, including rafts) may indeed speed up the encounters, whereas a disordered one may dramatically slow them down (Table 3). Thus, a paracrystalline structure and a disordered aggregation of R's with comparable concentrations may generate very different activation times, clearly favoring an ordered distribution.

Conclusions

Despite the fact that the phototransduction cascade in vertebrates is one of the most well understood signal transduction pathways mediated by GPCRs, and R is, to date, one of the two receptors whose structure is completely known, a lot of questions remain to be answered about the molecular mechanisms underlying each step making up the process. Our study suggests that the controversial molecular scenarios implied by recent AFM results may be compatible with the kinetics of R*−G encounters associated with the classical scenario. It is these interactions that are thought to set the rate of the photoresponse activation. In view of the increasing high-resolution experimental findings, which apparently contradict the pioneer studies from the 1970s, to be in doubt about the correctness of the classical picture appears at least fair. More importantly, new experiments aimed at directly determining D_G and D_R in vivo, for instance, would be extremely useful in order to clear up the actual scenario.

Acknowledgment. We are extremely grateful to Prof. Francesca Fanelli for helpful discussions. We further acknowledge the precious help from Dr. Paul Park who kindly provided us with useful experimental data concerning rhodopsin rafts.

References and Notes

(1) Baylor, D. A.; Lamb, T. D.; Yau, K. W. *J. Physiol.* **1979**, *288*, 613.
(2) Kahlert, M.; Hofmann, K. P. *Biophys. J.* **1991**, *59*, 375.
(3) Lamb, T. D.; Pugh, E. N., Jr. *J. Physiol.* **1992**, *449*, 719.
(4) Pugh, E. N., Jr.; Lamb, T. D. *Biochim. Biophys. Acta* **1993**, *1141*, 111.
(5) Pugh, E. N., Jr.; Lamb, T. D. *Phototransduction in Vertebrate Rods and Cones: Molecular Mechanisms of Amplification, Recovery and Light Adaptation*; Elsevier Science B.V.: Amsterdam/New York, 2000; Vol. 3.
(6) Felber, S.; Breuer, H. P.; Petruccione, F.; Honerkamp, J.; Hofmann, K. P. *Biophys. J.* **1996**, *71*, 3051.
(7) Lamb, T. D. *Biophys. J.* **1994**, *67*, 1439.
(8) Lamb, T. D. *Proc. Natl. Acad. Sci. U.S.A.* **1996**, *93*, 566.
(9) Laitko, U.; Hofmann, K. P. *Biophys. J.* **1998**, *74*, 803.
(10) Hamer, R. D.; Nicholas, S. C.; Tranchina, D.; Lamb, T. D.; Jarvinen, J. L. *Visual Neurosci.* **2005**, *22*, 417.
(11) Hamer, R. D.; Nicholas, S. C.; Tranchina, D.; Liebman, P. A.; Lamb, T. D. *J. Gen. Physiol.* **2003**, *122*, 419.
(12) Palczewski, K.; Kumasaka, T.; Hori, T.; Behnke, C. A.; Motoshima, H.; Fox, B. A.; Le Trong, I.; Teller, D. C.; Okada, T.; Stenkamp, R. E.; Yamamoto, M.; Miyano, M. *Science* **2000**, *289*, 739.
(13) Cherezov, V.; Rosenbaum, D. M.; Hanson, M. A.; Rasmussen, S. G.; Thian, F. S.; Kobilka, T. S.; Choi, H. J.; Kuhn, P.; Weis, W. I.; Kobilka, B. K.; Stevens, R. C. *Science* **2007**, *318* (5854), 1258−65.
(14) Fanelli, F.; De Benedetti, P. G. *Chem. Rev.* **2005**, *105*, 3297.
(15) Chabre, M.; Cone, R.; Saibil, H. *Nature* **2003**, *426*, 30.
(16) Fotiadis, D.; Liang, Y.; Filipek, S.; Saperstein, D. A.; Engel, A.; Palczewski, K. *Nature* **2003**, *421*, 127.
(17) Liang, Y.; Fotiadis, D.; Filipek, S.; Saperstein, D. A.; Palczewski, K.; Engel, A. *J. Biol. Chem.* **2003**, *278*, 21655.
(18) Cone, R. A. *Nat. New Biol.* **1972**, *236*, 39.
(19) Liebman, P. A.; Entine, G. *Science* **1974**, *185*, 457.
(20) Liebman, P. A.; Weiner, H. L.; Drzymala, R. E. *Methods Enzymol.* **1982**, *81*, 660.
(21) Bruckert, F.; Chabre, M.; Vuong, T. M. *Biophys. J.* **1992**, *63*, 616.
(22) Norisuye, T.; Hoffman, W. F.; Yu, H. *Biochemistry* **1976**, *15*, 5678.
(23) Okada, T.; Sugihara, M.; Bondar, A. N.; Elstner, M.; Entel, P.; Buss, V. *J. Mol. Biol.* **2004**, *342*, 571.
(24) Lambright, D. G.; Sondek, J.; Bohm, A.; Skiba, N. P.; Hamm, H. E.; Sigler, P. B. *Nature* **1996**, *379*, 311.
(25) Dell'Orco, D.; Seeber, M.; Fanelli, F. *FEBS Lett.* **2007**, *581*, 944.
(26) Nickell, S.; Park, P. S.; Baumeister, W.; Palczewski, K. *J. Cell Biol.* **2007**, *177*, 917.
(27) Saxton, M. J.; Owicki, J. C. *Biochim. Biophys. Acta* **1989**, *979*, 27.
(28) Calvert, P. D.; Govardovskii, V. I.; Krasnoperova, N.; Anderson, R. E.; Lem, J.; Makino, C. L. *Nature* **2001**, *411*, 90.
(29) Lamb, T. D.; Pugh, E. N., Jr. *Trends Neurosci.* **1992**, *15*, 291.
(30) Gupta, B. D.; Williams, T. P. *J. Physiol.* **1990**, *430*, 483.
(31) Hamm, H. E.; Bownds, M. D. *Biochemistry* **1986**, *25*, 4512.
(32) Kerov, V.; Rubin, W. W.; Natochin, M.; Melling, N. A.; Burns, M. E.; Artemyev, N. O. *J. Neurosci.* **2007**, *27*, 10270.
(33) Lamb, T. D.; Pugh, E. N., Jr. *Prog. Retin. Eye Res.* **2004**, *23*, 307.
(34) Lamb, T. D.; Pugh, E. N., Jr. *Invest. Ophthalmol. Visual Sci.* **2006**, *47*, 5137.
(35) Jastrzebska, B.; Fotiadis, D.; Jang, G. F.; Stenkamp, R. E.; Engel, A.; Palczewski, K. *J. Biol. Chem.* **2006**, *281*, 11917.
(36) Fanelli, F.; Dell'Orco, D. *Biochemistry* **2005**, *44*, 14695.
(37) Niu, S. L.; Mitchell, D. C. *Biophys. J.* **2005**, *89*, 1833.